Hindawi
Advances in Civil Engineering
Volume 2019, Article ID 2430652, 14 pages
https://doi.org/10.1155/2019/2430652

Research Article

Mechanical Properties of High-Strength High-Performance Reinforced Concrete Shaft Lining Structures in Deep Freezing Wells

Shilong Peng,[1] Chuanxin Rong,[1] Hua Cheng,[1,2] Xiaojian Wang,[1] Mingjing Li,[1] Bin Tang,[1] and Xuemei Li[1]

[1]*School of Civil Engineering and Architecture, Anhui University of Science and Technology, 168 Taifeng St, Huainan 232001, China*
[2]*School of Resources and Environmental Engineering, Anhui University, 111 Jiulong Rd, Hefei 230601, China*

Correspondence should be addressed to Chuanxin Rong; chxrong@aust.edu.cn

Received 9 November 2018; Revised 2 March 2019; Accepted 18 March 2019; Published 8 April 2019

Academic Editor: Chiara Bedon

As coal resources must be mined from ever deeper seams, high-strength, high-performance concrete shaft linings are required to resist the load of the soil surrounding the deep freezing well. In order to determine the optimal concrete mix for the unique conditions experienced by such high-strength high-performance reinforced concrete shaft lining (HSHPRCSL) structures in deep freezing wells, an experimental evaluation of scaled HSHPRCSL models was conducted using hydraulic pressure load tests. It was observed that as the specimens ruptured, plastic bending of the circumferential reinforcement occurred along the failure surface, generated by compression-shear failure. These tests determined that HSHPRCSL capacity was most affected by the ultimate concrete uniaxial compressive strength and the thickness-diameter ratio and least affected by the reinforcement ratio. The experimental results were then used to derive fitting equations, which were compared with the results of theoretical expressions derived using the three-parameter strength criterion for the ultimate bearing capacity, stress, radius, and load in the elastic and plastic zones. The proposed theoretical equations yielded results within 8% of the experimentally fitted results. Finally, the finite element analysis method is used to verify the abovementioned results, and all errors are less than 12%, demonstrating reliability for use as a theoretical design basis for deep HSHPRCSL structures.

1. Introduction

As the more accessible portions of coal resources near the surface are gradually depleted in large coal producing Chinese provinces such as Hebei, Henan, Shandong, and Anhui, it is necessary to mine deeper coal seams. As mines are constructed deeper, the alluvium traversed by the shaft lining becomes thicker and thicker. For example, the Wanfu Mine, currently under construction at the Juye Coalfield in Shandong, and the Kouzixi Mine, being planned for the Zhangou Coalfield in Anhui, will traverse 600–800 m of overlying ground. This, naturally, results in an increase in the ground pressure acting on the shaft lining. To resist strong frost heave pressure and permanent load acting on the freezing shaft lining in such deep alluvium, it is necessary to provide a high-strength shaft lining structure [1, 2]. According to the theory of shaft lining structural design, the primary method of improving the ultimate bearing capacity of a freezing shaft lining is to increase the thickness of the shaft lining, use steel plate on the inside face of the lining as a concrete restraint structure, or cast the shaft using high-strength concrete. Among these options, the most effective measure is to increase the concrete strength in the shaft lining by using high-strength, high-performance concrete (HSHPC) [3], such as grades C60 to C80, in the design of the deep freezing shaft lining structure.

Although C60–C80 grade HSHPC has been used in China in bridge, water conservation, and high-rise building projects, the construction environment and performance requirements of these HSHPCs are quite different from those

required of deep-alluvium freezing shaft lining concrete. Because the thickness of the inner and outer shaft lining increases from about 0.7 m in shallow strata to about 1.2 m in deep strata, the use of HSHPC in these deep structures is classified as a mass concrete project, and accordingly the control of cracking is a significant challenge during the construction process. To ensure the safety of the wellbore as it is sunk to such depths, the average design temperature of the freezing wall is reduced from about −10°C to about −15°C. As the temperature of the freezing wellbore is decreased, the difference between the internal and external temperature of the shaft lining concrete increases, resulting in a deterioration of the concrete curing environment. Generally, when constructing a shaft lining in deep alluvium using a freezing wellbore, the concrete should have high strength, high impermeability, and good workability [4]. Therefore, to ensure that the HSHPC mix ratio used in shaft construction is economical, reasonable, and reliable, it is essential to conduct research on the preparation and behaviour of HSHPC in deep freezing wells.

Domestic and foreign scholars alike have conducted a great deal of research into concrete shaft linings [5–10], but there has been little research into the mechanical properties of a high-strength, high-performance reinforced concrete shaft lining (HSHPRCSL) structure, and most of this existing research has been mainly experimental [3, 11–14]. Yang derived a practical equation for the radial and vertical bearing capacity of a concrete shaft lining using the results of a destructive testing program of concrete shaft lining models and expressed the concrete strength criterion for the inner face of the shaft lining in a form similar to the Coulomb shear strength criterion equation [7]. Rong et al. obtained an experimental regression equation for the ultimate bearing capacity of a shaft lining using the experimental results of shaft lining model tests and analysed the mechanical properties of the shaft lining structure using the Mohr–Coulomb strength criterion [14]. Assuming that the external load is not too large, it is often more practical to analyse the mechanical properties of shaft lining concrete using the Mohr–Coulomb criterion, but it has been found that the mechanical properties of concrete under multiaxial stress should be considered under large external loads [15]. Indeed, the vertical shaft lining of a coal mine shaft constructed using the freezing method in deep alluvium generally adopts a double-layer shaft lining structure type in which the concrete of the inner shaft lining of the freezing well is generally in a bi- or tridirectional stress state [16–18]. Because the three-parameter strength criterion [19–22] considers the influence of multiaxial stress, it is better equipped to reflect the mechanical properties of an HSHPRCSL under multiaxial stress.

In view of the current state of HSHPRCSL research and according to the special curing environment and construction conditions of deep freezing shaft linings, in this study, the qualities of different mix ratios are evaluated in preparation tests of C60–C80 HSHPC to obtain an optimal mix. According to the stress characteristics of the inner shaft lining of a deep freezing well, the mechanical properties and failure characteristics of the HSHPRCSL structure are then studied using model tests and theoretical calculations. A three-parameter strength criterion conforming to the strength characteristics of the concrete is then adopted to derive an analytical expression for the ultimate bearing capacity and stress distribution in the elastic and plastic zones of an HSHPRCSL structure. Finally, the finite element analysis method is used to verify the abovementioned results. The resulting conclusions provide a design basis for the engineering application of HSHPC in deep freezing shaft lining structures.

2. Evaluation of HSHPC Mixes

2.1. Objectives of HSHPC Preparation. High-strength, high-performance concrete possesses excellent properties before and after hardening that are provided by mixing a fine active admixture and high-efficiency compound water-reducing agent under conditions of low cement content and low water-cement ratio. These properties generally include high workability, high impermeability, high volume stability (no cracking during hardening and smaller shrinkage and creep), high strength (above C30 grade), the maintenance of continuous growth in long-term strength, and ultimately excellent durability when subjected to a harsh environment. In view of the special curing environment and construction conditions of the inner shaft lining of a freezing shaft in deep alluvium, the inner shaft lining concrete should possess high strength, crack resistance, seepage prevention, and high early strength to prevent leakage of the shaft lining after the thawing of the frozen wall. Therefore, the preparation of HSHPC for an inner shaft lining should address the following principle qualities:

(i) Ultrahigh early strength with which concrete can be demoulded 10 hours after pouring
(ii) Simple preparation process
(iii) Good workability and a slump greater than 180 mm, which is convenient for transportation and pouring
(iv) Low hydration heat and high durability
(v) High volume stability and high impermeability

2.2. Preparation of HSHPC. Various factors affecting the strength, fluidity, and durability of HSHPC include the variety and dosage of cement, the mix ratio of the concrete, the variety and dosage of admixtures and externally mixed active materials, the aggregate gradation, the construction process, and the environmental conditions at the site. In general, the common mix for grade C60 HSHPC and above consists of a high-grade cement, superplasticiser (with a water reduction rate greater than or equal to 35%), mineral admixture, high quality aggregate, and controlled sand content.

2.3. Selection of Raw Materials for HSHPC

2.3.1. Cement. The C60–C80 HSHPC evaluated in this study used Conch brand P.O. 42.5R and P.O. 52.5R early strength ordinary Portland cement with lower relative hydration heats, produced by Ningguo Cement Factory. The early

strength and low heat of hydration properties of this cement make it especially suitable for the preparation of HSHPC for use in freezing shaft linings in deep alluvium.

2.3.2. Aggregate. The fine aggregate used in this study was Huaibin medium sand from Henan Province with a fineness modulus of 2.9, a bulk density of 1540 kg/m^3, and a mud content of 1.6%. The coarse aggregate used was Shangyao limestone gravel from Huainan City and Mingguang basalt from Chuzhou City, both in Anhui Province, which have a crushing index of 8.3% and 3.3%, respectively, and a continuous grain size grade of 5–31.5 mm.

2.3.3. Water Reducing Agent. In consideration of the special use environment of HSHPC in shaft linings, it is critical that an admixture be selected that provides excellent performance with the raw materials in the mix. A compatibility test was accordingly conducted by evaluating eight types of high-efficiency composite water-reducing agents (superplasticisers). In the end, an NF naphthalene-based superplasticiser produced by Huainan Mining Group Synthetic Material Co., Ltd., was selected for use in the experiments due to its good compatibility with the other materials in the mix.

2.3.4. Mineral Admixture. The mineral admixtures used in the experiments were a silicon powder produced by Shanxi Dongyi Ferroalloy Factory, a ground slag produced by Hefei Iron and Steel Group of Jinjiang Building Materials Co., Ltd., and a Grade I fly ash produced by Huainan Pingwei Power Plant. The main chemical components of the silicon powder and ground slag are provided in Table 1.

The type of silicon powder used in this study contained extremely fine particles consistent with an ultrafine solid material with ultrafine characteristics. The SiO_2 content of the silicon powder was greater than 90%, its average particle size was 0.1–0.15 μm, its minimum particle size was 0.01 μm, and particles of less than 1 μm accounted for more than 80% of the powder. The specific surface area was 250 000–350 000 cm^2/g, which is 70–90 times that of cement. The specific gravity was 2.1–3.0 g/cm^3, and the bulk density was 200–250 kg/m^3. The specific surface area of the ground slag was 3800 cm^2/g. The water demand ratio of the fly ash was 89%, its loss on ignition was 0.95%, its SO_3 content was 0.29%, and its fineness was 4%.

2.4. Compressive Strength Test Results for HSHPC Mixes. According to the specification for the design of concrete mixes, the mixing strengths of C60, C65, C70, C75, and C80 concrete are 69.8, 74.8, 79.8, 84.8, and 89.8 MPa, respectively. Using the orthogonal testing method, the C60–C80 concrete mix proportions shown in Table 2 were evaluated for application in freezing shaft linings.

Compressive strength tests were conducted on the mixes detailed in Table 2 with the results shown in Table 3, in which it can be seen that the three-day compressive strengths of the mixes reached 80% of the design value, the seven-day compressive strengths reached 90% of the design value, and the twenty-eight-day compressive strengths met or exceeded the design strength. These results indicate that that proposed mixes are able to fully meet the strength and performance requirements of the HSHPRCSL.

Table 1: Chemical composition of silicon powder and ground slag (%).

Component	SiO_2	Al_2O_3	Fe_2O_3	CaO	MgO	SO_3
Silicon powder	92.6	0.78	0.59	0.8	1.0	0.81
Ground slag	35.3	8.93	1.26	42.2	6.9	2.0

3. HSHPRCSL Model Test Method

3.1. Similarity Principle of Model Test. Given the high-strength and large size of an HSHPRCSL structure, destructive tests on a prototype shaft lining were determined to be prohibitively difficult to implement. As a result, scale models of a shaft lining structure were tested in this study.

The objective of the model tests was not only to determine the stress distribution within the shaft lining section but also to measure the failure load of the shaft lining. Therefore, the shaft lining model design must not only be subjected to scaled stress and deformation but also to a scaled load via a similarity index. Using similarity theory and the basic equations of elasticity, this study applied the equation analysis method [23] to determine the similarity index of the shaft lining model.

The similarity conditions of the stress and deformation in the shaft lining model can be obtained from the geometric equations, boundary equations, and physical equations as follows:

$$\begin{cases} \dfrac{C_\varepsilon C_l}{C_\delta} = 1, \\ \dfrac{C_p}{C_\sigma} = 1, \\ \dfrac{C_E C_\varepsilon}{C_\sigma} = 1, \\ C_\nu = 1, \end{cases} \tag{1}$$

where C_ε is the strain similarity constant; C_l is the geometric similarity constant; C_δ is the displacement similarity constant; C_p is the load (surface force) similarity constant; C_E is the elastic modulus similarity constant; C_σ is the stress similarity constant; and C_ν is Poisson's ratio similarity constant.

The HSHPRCSL is a composite structure composed of two materials, steel and concrete, so in order to ensure that the stress and deformation of each component of the model and the prototype are strictly comparable, it is necessary to maintain geometric similarity between the model and prototype of shaft lining before, throughout, and after loading and deformation; accordingly, $C_l = C_\delta$ and $C_\varepsilon = 1$. Therefore, the stress and strain conditions in the shaft lining can be written as

Table 2: Mix ratios of C60, C65, C70, C75, and C80 HSHPC.

Specimen number	Strength grade	Cement : sand : stone : water : mineral admixture (kg)	Cementitious materials (kg)	Water-binder ratio	Sand ratio (%)	Admixture dosage (%)
1	C60	410 : 628.0 : 1166.3 : 151.2 : 130	540	0.280	35	NF1.8
2	C65	410 : 625.5 : 1161.6 : 152.6 : 145	555	0.275	35	NF1.8
3	C70	410 : 620.0 : 1151.4 : 145.6 : 150	560	0.260	35	NF1.9
4	C75	420 : 622.5 : 1156.1 : 144.1 : 145	565	0.255	35	NF2.0
5	C80	430 : 616.6 : 1145.1 : 146.3 : 155	585	0.250	35	NF2.0

Table 3: HSHPC strength test results.

Specimen number	Design strength grade	Slump (mm)	Compressive strength of cube specimen (MPa)		
			3 d	7 d	28 d
1	C60	206	57.6	63.7	70.4
2	C65	213	60.7	69.8	75.8
3	C70	195	64.2	72.7	79.5
4	C75	210	69.5	78.2	85.3
5	C80	205	73.2	81.4	90.1

$$\begin{cases} \dfrac{C_l}{C_\delta} = 1, \\ \dfrac{C_p}{C_\sigma} = 1, \\ \dfrac{C_E C_\varepsilon}{C_\sigma} = 1. \end{cases} \tag{2}$$

In order to ensure that the load and shape of the shaft lining model are identical to those of the prototype at the time of failure, the stress-strain behaviour of the model in the elastic state must be similar to that of the prototype in the elastic state. Accordingly, the following strength requirements should be met:

(i) The stress-strain curves of the shaft lining model and prototype should be similar throughout the loading process

(ii) The strength of the materials in each part of the shaft lining should be similar to each other

(iii) The strength criteria for the damage of the model and prototype shaft lining should be similar

To fully meet the required conditions of similarity, it is preferable that the materials proposed for the prototype shaft lining structure be used in the model test. Therefore, the structural material of the shaft lining model was adjusted in the experiment as follows:

$$\begin{cases} C_E = C_\sigma = C_p = C_R = 1, \\ C_\varepsilon = 1, \\ C_\mu = 1, \end{cases} \tag{3}$$

where C_R is the strength similarity constant and C_μ is the reinforcement ratio similarity constant.

In this case, the appropriate geometric similarity constant is the only variable that needs to be determined. In order to make the study results universal, instead of using a specific shaft lining as the simulation object, the simulation was concerned with the effects of the thickness-diameter ratio λ, a dimensionless quantity with a similarity constant equal to 1. Model tests of three different shaft lining thicknesses were accordingly conducted with λ values of 0.219, 0.216, and 0.201. In consideration of the size of the test loading device and the characteristics of the shaft lining structure of the main shaft of the Jixi Shengjian coal mine in Shandong and the auxiliary shaft of the Huainan Dingji coal mine in Anhui, the shaft lining model parameters were obtained from an orthogonal design table [24] and are shown in Table 4. The geometry of the shaft lining model is shown in Figure 1, in which the outer diameter and height of the model are 925.0 mm and 562.5 mm, respectively, and the thickness is varied by changing the inner diameter.

3.2. Model Loading. To ensure good quality, the shaft lining models were cast using professional formwork. To provide consistent boundary conditions under load, the top and bottom faces of the model were processed using a lathe to obtain a high finish after pouring. The shaft lining model loading tests were conducted using a high-load hydraulic loading device, shown in Figure 2, to maintain a constant load simulating the uniform ground pressure, as shown in the schematic in Figure 3. The load test was conducted by first applying a preload two to three times before increasing the load in stable pressure increments, each held for 5–10 minutes while measured data were recorded, until the model exhibited damage.

3.3. Measurement Method. The compressive strengths of the HSHPC mixes were determined by three standard cube compression tests for each model mix, with the average values reported in Table 4. The load applied to the

Table 4: Model parameters.

Model	a (mm)	b (mm)	λ	μ (%)	σ_{cm} (MPa)
A-1	380.5	462.5	0.216	0.9	65.3
A-2	380.5	462.5	0.216	1.2	72.2
A-3	380.5	462.5	0.216	0.6	76.8
A-4	385	462.5	0.201	1.38	67.9
A-5	385	462.5	0.201	1.38	74.2
A-6	385	462.5	0.201	1.38	79.3
A-7	379.5	462.5	0.219	0.7	62.2
A-8	379.5	462.5	0.219	0.7	78.3

Note: a is the inner radius; b is the outer radius; λ is the thickness-diameter ratio, where $\lambda = (b - a)/a$; μ is the reinforcement ratio; and σ_{cm} is the average cube compressive strength.

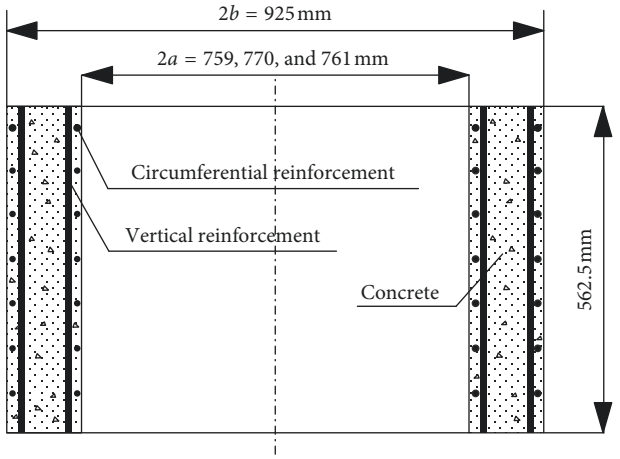

Figure 1: Shaft lining structure model (unit: mm).

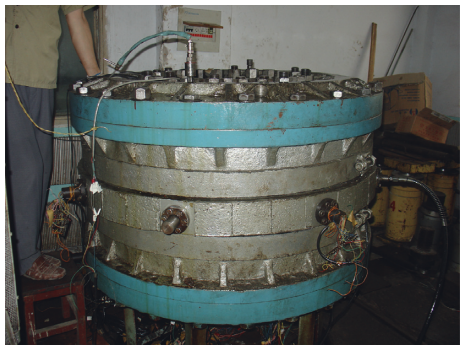

Figure 2: Shaft lining model loading device.

HSHPRCSL model was measured using the standard pressure gauge installed on the high-pressure loading device and a BPR oil pressure sensor. Measurements of the strain in the shaft lining model were conducted using resistance strain gages arranged on the inner and outer surfaces of the concrete models and on the inner and outer rows of reinforcing bars, as shown in Figures 4 and 5. Two levels of gages were located vertically along the shaft lining model, and each layer contained four measurement points arranged in the circumferential direction. The load and strain in the shaft lining were collected and processed in real time by the test system. During the test, the system used the oil pressure sensor to determine the load in order to ensure that the load cell voltage regulation error was within the allowable range.

3.4. Concrete Strength Data Processing

3.4.1. Standard Value of Cube Compressive Strength. According to the Code for the Design of Concrete Structures [25], the concrete strength grade should be determined according to the standard 150-mm cube compressive strength, σ_c, obtained by testing using the standard test method at an age of 28 days or whatever age is required by the design. After statistical analysis, the compressive strength of the concrete can be approximately taken as a normal distribution, as shown in Figure 6, such that the average cube compressive strength provides 95% accuracy.

If the total area under the curve in Figure 6 is taken as 1 and the area on both sides of the average value κ is 50%, using $\kappa - 1.645\sigma = (1 - 1.645\delta)\kappa$ as the line of demarcation, the area to the left and right should be 5% and 95%, respectively. Using these statistical characteristics, the relationship between the standard cube compressive strength σ_c and the average compressive strength σ_{cm} can be obtained as follows:

$$\sigma_c = (1 - 1.645\delta)\sigma_{cm}, \tag{4}$$

where δ is the coefficient of variation of the concrete strength according to the statistics of the test results and can be determined by interpolation from the numerical values provided in Table 5.

3.4.2. Axial Compressive Strength. Considering the difference between the actual strength of the HSHPRCSL and the concrete strength determined by the cube test, past experience, and test data analysis and in reference to the relevant design code provisions of other countries [26], the strength of the concrete structure design should be corrected based on the concrete strength of the specimen. In this study, the correction coefficient was set to 0.88.

The ratio of prism compressive strength to axial compressive strength, α_{c1}, for ordinary concrete (less than or equal to C50) is $\alpha_{c1} = 0.76$, while for high-strength concrete (C80), it is $\alpha_{c1} = 0.82$. When the concrete strength grade is between C50 and C80, linear interpolation is used to determine the appropriate ratio.

Because high-strength concrete is more brittle than conventional concrete, in order to ensure the safety of the structure, a brittleness reduction factor, α_{c2}, has been introduced in the specification. For ordinary concrete (less than or equal to C40), $\alpha_{c2} = 10$, while for high-strength concrete (C80), $\alpha_{c2} = 0.87$. When the concrete strength grade is between C40 and C80, linear interpolation is used to determine the ratio.

According these provisions, the standard value of the concrete axial compressive strength can be obtained as follows, with the results shown in Table 6:

$$\sigma_y = 0.88\alpha_{c1}\alpha_{c2}\sigma_c = 0.88\alpha_{c1}\alpha_{c2}(1 - 1.645\delta)\sigma_{cm}. \tag{5}$$

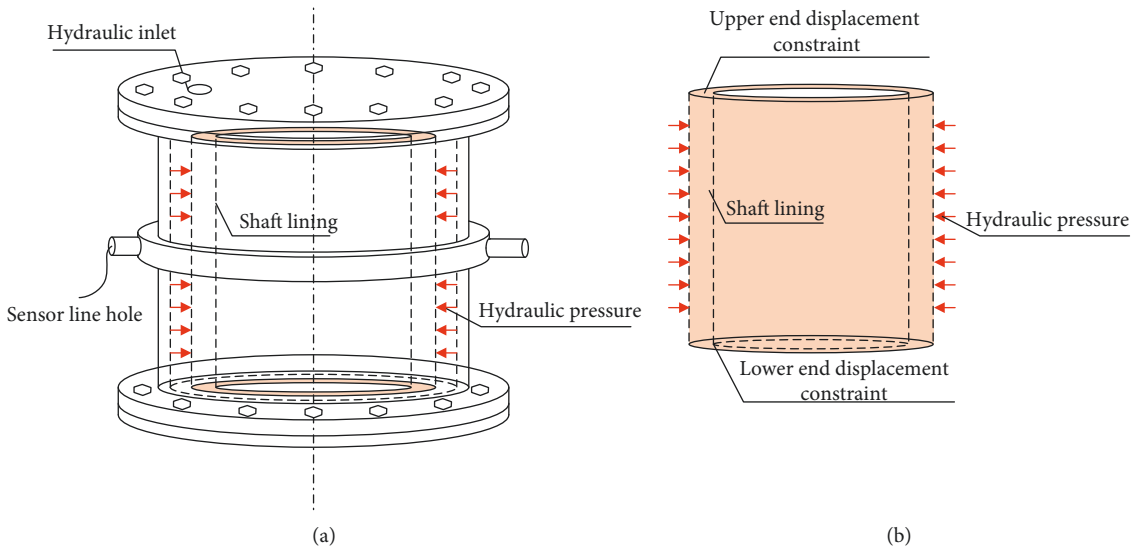

Figure 3: Schematic diagram of shaft lining model loading device.

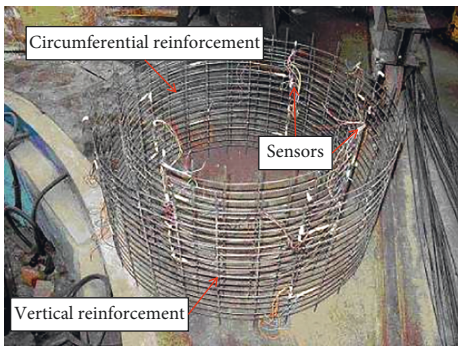

Figure 4: Layout of reinforcing mesh and measurement points of shaft lining model.

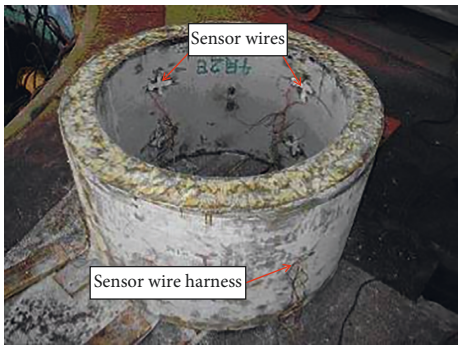

Figure 5: Shaft lining model and concrete surface measurement points.

3.4.3. Axial Tensile Strength. The standard axial tensile strength σ_1 is calculated as follows, with the results shown in Table 7:

$$\sigma_1 = 0.88 \times 0.395\sigma_c^{0.55}(1 - 1.645\delta)^{0.45} \times \alpha_{c2}, \quad (6)$$

where the coefficient of 0.395 and the exponent of 0.55 represent the relationship of axial tensile strength to the cube

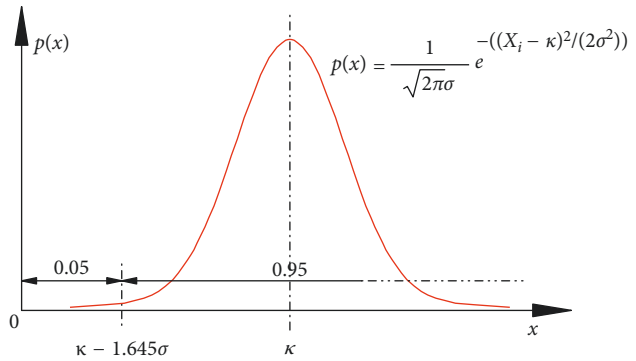

Figure 6: Normal distribution of concrete compressive strength.

compressive strength, determined by statistical analysis of the test data.

3.4.4. Biaxial Compressive Strength. The biaxial strength envelope of the concrete is a closed curve composed of four segments, shown in Figure 7, each of which expresses tensile stress as negative and compressive stress as positive, determined according to the quadrant in which the segment is located. The strength envelope curve can be described by the following equations:

$$\begin{cases} L_1 : f_1^2 + f_2^2 - 2\nu f_1 f_2 = \sigma_1^2, \\ L_2 : \sqrt{f_1^2 + f_2^2 - f_1 f_2} - \alpha_s (f_1 + f_2) = (1 - \alpha_s)\sigma_y, \\ L_3 : \dfrac{f_2}{\sigma_y} - \dfrac{f_1}{\sigma_1} = 1, \\ L_4 : \dfrac{f_1}{\sigma_y} - \dfrac{f_2}{\sigma_1} = 1, \end{cases} \quad (7)$$

Table 5: Coefficient of variation of concrete strength (%) [25].

Strength grade	C15	C20	C25	C30	C35	C40	C45	C50	C55	C60–C80
δ	23.3	20.6	18.9	17.2	16.4	15.6	15.6	14.9	14.9	14.1

Table 6: Standard value of axial concrete compressive strength (MPa) [25].

Strength grade	C15	C20	C25	C30	C35	C40	C45	C50	C55	C60	C65	C70	C75	C80
σ_y	10.0	13.4	16.7	20.1	23.4	26.8	29.6	32.4	35.5	38.5	41.5	44.5	47.4	50.2

Table 7: Standard value of axial concrete tensile strength (MPa) [25].

Strength grade	C15	C20	C25	C30	C35	C40	C45	C50	C55	C60	C65	C70	C75	C80
σ_l	1.27	1.54	1.78	2.01	2.20	2.39	2.51	2.64	2.74	2.85	2.93	2.99	3.05	3.11

where α_s is the shear yield parameter, determined by $\alpha_s = (r-1)/(2r-1)$; r is the increase coefficient of biaxial compressive strength, ranging from 1.13 to 1.15, determined by experimental data and taken as 1.2 in the absence of experimental data; f_i is the representative value of the multiaxis concrete strength; $f_1 \geq f_2 \geq f_3$; and ν is Poisson's ratio of the concrete, taken in the range of 0.18–0.22.

For convenience of calculation, the biaxial compressive strengths indicated in Figure 7 can be interpolated according to the data in Table 8.

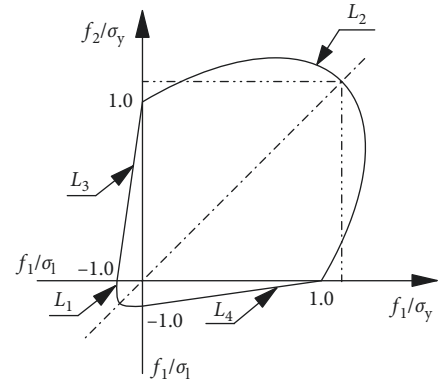

Figure 7: Strength envelope diagram of biaxial stress in concrete.

4. Results of HSHPRCSL Model Tests

4.1. Ultimate Bearing Capacity of HSHPRCSL. The experimentally determined ultimate bearing capacities (P_b) of the shaft lining models are provided in Table 9, in which it can be seen that, under the action of a uniformly distributed load, the HSHPRCSL models exhibit a high bearing capacity, providing a reasonable solution to the issues of supporting shafts in deep alluvium. Through a regression analysis of the test results in Table 9, the regression formula for the ultimate bearing capacity of HSHPRCSL structures can be obtained as follows:

$$P_b = 0.557\sigma_c^{1.272}\lambda^{0.917}\mu^{0.0302}, \quad (8)$$

which indicates that the ultimate bearing capacity (P_b) of the shaft lining is mainly related to the standard concrete cube compressive strength (σ_c), thickness-diameter ratio (λ), and the reinforcement ratio (μ).

In order to provide a reasonable and economic shaft lining design, the relationships between bearing capacity and reinforcement ratio and between bearing capacity and concrete compressive strength (Figures 8 and 9, respectively) were determined using empirical equation (8). Under the action of a uniformly distributed load, the power exponent of the reinforcement ratio (μ) was accordingly determined to be 0.0302, very close to 0, indicating that an increase in the reinforcement ratio has only a very small effect on the ultimate bearing capacity of the HSHPRCSL models. As shown in Figure 8, for the same concrete strength grade, an increase in the reinforcement ratio from 0.3% to 0.8% results in only an approximately 0.85 MPa improvement in the ultimate bearing capacity while requiring a significant increase in the quantity of reinforcing bars. This not only increases the project cost but also makes underground concrete vibration very difficult, adversely affecting the quality of the poured concrete. Therefore, improving the ultimate bearing capacity of the shaft lining by increasing the reinforcement ratio is unreasonable. Due to the insignificant influence of the reinforcement ratio on the ultimate bearing capacity of the models, the contribution of the reinforcement ratio to the ultimate bearing capacity of the reinforced concrete shaft lining is not considered in the following theoretical analysis of the ultimate bearing capacity.

The ultimate bearing capacity of the HSHPRCSL model was found to be significantly influenced by the strength grade of the concrete. Figure 9 indicates that an increase of 10 MPa in the concrete strength grade raised the ultimate bearing capacity of the model by about 6.29 MPa. An increase in the thickness-diameter ratio was also observed to improve the ultimate bearing capacity of the model: at C60, an increase in the thickness-diameter ratio from 0.2 to 0.3 raised the ultimate bearing capacity of the model by about 8.87 MPa. Combined with an increase in concrete strength grade, the effect of an increase in the thickness-diameter

Table 8: Compressive strength of concrete under biaxial compression [25].

f_1/σ_y	1.0	1.05	1.10	1.15	1.20	1.25	1.29	1.25	1.20	1.16
f_2/σ_l	0	0.07	0.16	0.25	0.36	0.50	0.88	1.03	1.11	1.16

Table 9: Comparison of theoretically, experimentally, and numerically determined HSHPRCSL plastic ultimate bearing capacity.

Model	σ_{cm} (MPa)	σ_c (MPa)	σ_y (MPa)	σ_l (MPa)	σ_{2y} (MPa)	P_{b1} (MPa)	P_{b2} (MPa)	P_{b3} (MPa)
A-1	65.3	49.19	31.85	2.62	40.26	17.0	17.51	18.72
A-2	72.2	54.98	35.44	2.74	44.79	19.5	20.25	21.82
A-3	76.8	58.87	37.82	2.83	47.80	21.0	22.08	22.40
A-4	67.9	51.38	33.21	2.67	41.98	16.8	16.99	17.50
A-5	74.2	56.67	36.48	2.78	46.11	19.0	19.29	20.87
A-6	79.3	61.01	39.12	2.87	49.45	21.0	21.21	23.01
A-7	62.2	46.45	30.13	2.55	38.08	15.5	16.58	16.95
A-8	78.3	60.14	38.59	2.85	48.78	21.5	23.13	23.88

Note: σ_{cm} is the average cube compressive strength; σ_c is the standard cube compressive strength; σ_y is the prismatic axial compressive strength; σ_l is the prismatic axial tensile strength; σ_{2y} is the biaxial compressive strength; P_{b1} is the experimentally determined ultimate bearing capacity; P_{b2} is the theoretically determined ultimate bearing capacity; and P_{b3} is the numerically determined ultimate bearing capacity.

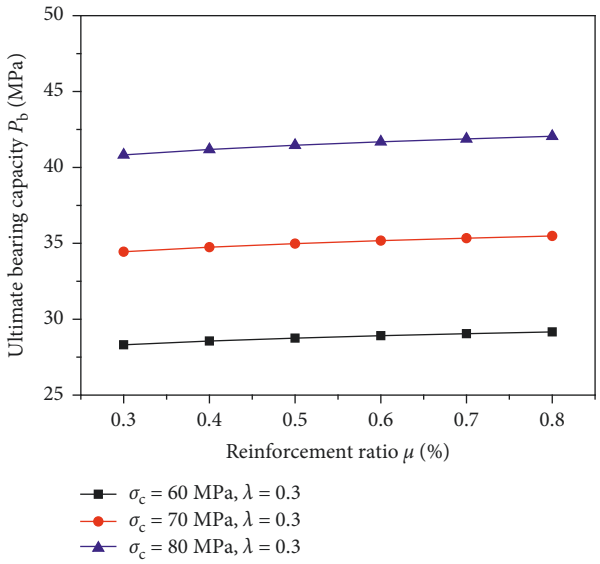

Figure 8: Relationship curve between ultimate bearing capacity and reinforcement ratio.

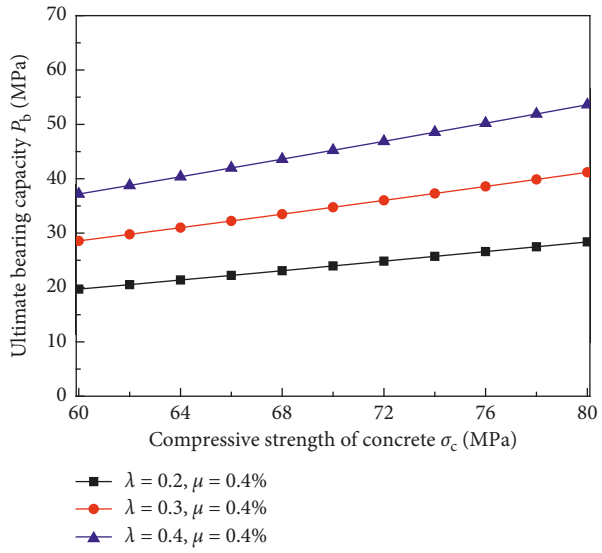

Figure 9: Relationship between ultimate bearing capacity and concrete compressive strength.

ratio on the increase in bearing capacity would be even more noticeable. For C80 concrete, an increase in the thickness-diameter ratio from 0.2 to 0.3 raises the ultimate bearing capacity of the HSHPRCSL model by about 12.79 MPa. However, in reality, increasing the thickness-diameter ratio is often limited by engineering conditions; therefore, the ultimate bearing capacity of HSHPRCSL is most effectively improved by increasing the strength of the concrete during the design stage.

4.2. HSHPRCSL Model Failure Modes. Figure 10 depicts the typical observed failure mode of the HSHPRCSL models. When the external load on the shaft lining was fairly large, the circumferential stress in the interior face of the shaft concrete reached its ultimate strength first. As the direction of free deformation is normal to the inner face, these surfaces of the models exhibited very small inclined cracks and local peeling at this time. As the applied load was increased, the high stress area in which the ultimate strength had been exceeded rapidly spread from the inner face to the outer face of the model, and compression and shear failure eventually occurred in the portion of the shaft lining in which the concrete was the weakest, forming a failure surface running through the entire thickness of the shaft lining model. When failure occurred, large chunks of concrete were observed to fall, inclined broken cracks appeared, and the circumferential bars bent plastically along the failure surface. The angle between the failure surface and the maximum principle stress was between 25 and 30°, suggesting a compressive shear failure.

(a) (b)

Figure 10: Shaft lining model failure mode.

5. Theoretical Analysis of HSHPRCSL Based on the Three-Parameter Strength Criterion

5.1. Three-Parameter HSHPC Strength Criterion. The failure surface of the three-parameter strength criterion, shown in Figure 11, is smooth as its meridian is a parabola, a significant improvement over conventional strength criteria. The three-parameter strength criterion is usually expressed in terms of uniaxial tensile strength, uniaxial compressive strength, and biaxial compressive strength, represented by σ_l, σ_y, and σ_{2y}, respectively [19], using as a combination of stresses ρ, ξ, and θ, defined by

$$\begin{cases} \rho = \sqrt{2J_2}, \\ \xi = \dfrac{1}{\sqrt{3}} I_1, \\ \cos 3\theta = \dfrac{3\sqrt{3}\, J_3}{2\sqrt{J_2^3}}, \quad 0 \le \theta \le 60^\circ, \end{cases} \tag{9}$$

where $I_1 = \sigma_1 + \sigma_2 + \sigma_3 = 3\sigma_m$, $J_2 = 1/6[(\sigma_1 - \sigma_2)^2 + (\sigma_2 - \sigma_3)^2 + (\sigma_3 - \sigma_1)^2]$, and $J_3 = s_1 s_2 s_3 = (\sigma_1 - \sigma_m)(\sigma_2 - \sigma_m)(\sigma_3 - \sigma_m)$.

For the yield plane of the three-parameter strength criterion shown in Figure 11, any point $M(\rho, \xi, \theta)$ on the failure plane can be defined by

$$M(\rho, \xi, \theta) = \rho^2 + A_1(\theta)\rho + A_2(\theta)\xi + A_3(\theta) = 0, \tag{10}$$

where $A_1(\theta) = 1/2(a_1 + a_2) + 1/2(a_2 - a_1)\cos 3\theta$, $A_2(\theta) = 1/2(b_1 + b_2) + 1/2(b_2 - b_1)\cos 3\theta$, $A_3(\theta) = -\sqrt{3}[1/2(b_1 + b_2) + 1/2(b_2 - b_1)\cos 3\theta]\sigma_l$, $a_1 = (\sqrt{6}/9)(K_y^2 - K_y - 3)\sigma_l$, $a_2 = (\sqrt{6}/9)(2K_{2y}^2 - 2K_{2y} - 3)\sigma_l$, $b_1 = (2\sqrt{3}/9)K_y(K_y - 1)\sigma_l$, $b_2 = (2\sqrt{3}/9)K_{2y}(K_{2y} - 1)\sigma_l$, and $K_y = \sigma_y/\sigma_l$, $K_{2y} = \sigma_{2y}/\sigma_l$.

5.2. Mechanical Model. Because the shaft lining is under external pressure, the principle stress components σ_r, σ_θ, and σ_z, defined as the radial stress, hoop stress, and vertical stress, respectively, are all negative as they are compressive such that $0 > \sigma_r > \sigma_z > \sigma_\theta$. Supposing that a and b are the inner and outer radii of the shaft lining, respectively, under the action of external pressure, the shaft lining is in a state of elastic-plastic behaviour, where r_p, determined and applied later in this section, denotes the radius of the elastic-plastic boundary (as illustrated in Figure 12).

5.3. Analysis of Elastic-Plastic Behaviour and Ultimate Bearing Capacity of HSHPRCSL Structures. Mine shaft lining can be analysed as a plane axially symmetric problem in which the radial stress σ_r and hoop stress σ_θ are only a function of r, having nothing to do with θ such that $\sigma_r = \sigma_r(r)$ and $\sigma_\theta = \sigma_\theta(r)$. The intermediate principal stress is thus determined by $\sigma_z = \beta/2(\sigma_r + \sigma_\theta)$, where the intermediate principal stress coefficient β is defined as $0 \le \beta \le 1$. In the plastic zone, $\beta = 1$, making $\sigma_1 = \sigma_r$, $\sigma_3 = \sigma_\theta$, and $\sigma_2 = (\sigma_r + \sigma_\theta)/2$. Previously published work [27] has demonstrated that when the externally applied load p is very small, the shaft is in the elastic stage, with the stress components being defined as

$$\begin{cases} \sigma_r = -\dfrac{b^2 p}{b^2 - a^2}\left(1 - \dfrac{a^2}{r^2}\right), \\ \sigma_\theta = -\dfrac{b^2 p}{b^2 - a^2}\left(1 + \dfrac{a^2}{r^2}\right). \end{cases} \tag{11}$$

As p gradually increases, the stress in the inner shaft lining ($r = a$) reaches the concrete strength first, entering the plastic zone. This external load is defined as the elastic limit stress, denoted as p_e and determined as follows:

$$p_e = \frac{(b^2 - a^2)}{4b^2}\left[-(\sqrt{2}\,A_1 - \sqrt{3}\,A_2) + \sqrt{(\sqrt{2}\,A_1 - \sqrt{3}\,A_2)^2 - 8A_3}\right]. \tag{12}$$

When the external load $p > p_e$, the shaft lining enters the elastic-plastic stage, the plastic zone ($a \le r \le r_p$) begins to appear on the inner face of the shaft lining, and as p continues to increase, the plastic zone gradually extends outward. Because of axial symmetry, there is only the load q on the interface between the elastic and plastic zones, where $\sigma_r|_{r=r_p} = -q$, and r_p is the radius of the elastic-plastic boundary, shown in Figure 12. In the plastic zone, the stress component is satisfied by

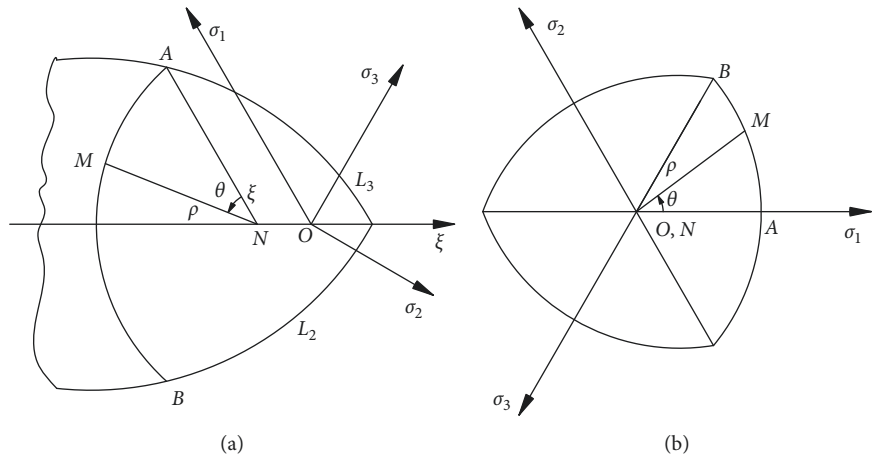

Figure 11: Parabolic three-parameter strength criterion.

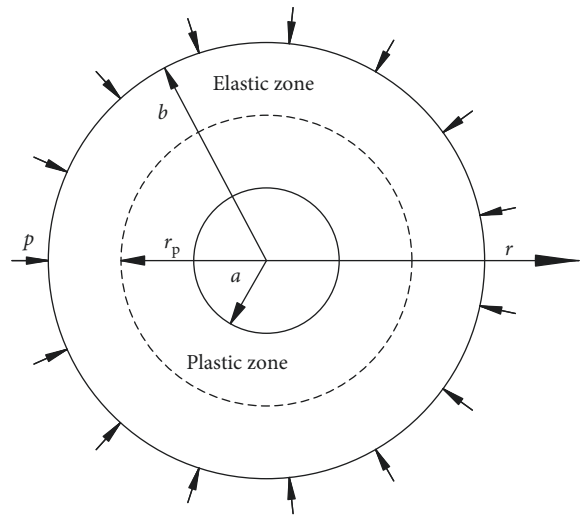

Figure 12: Mechanical model of concrete shaft lining.

$$\begin{cases} \sigma_r = -\dfrac{1}{\sqrt{3}\,A_2}\rho^2(r) + \left(\dfrac{1}{\sqrt{2}} - \dfrac{A_1}{\sqrt{3}\,A_2}\right)\rho(r) - \dfrac{A_3}{\sqrt{3}\,A_2}, \\ \sigma_\theta = -\dfrac{1}{\sqrt{3}\,A_2}\rho^2(r) - \left(\dfrac{1}{\sqrt{2}} + \dfrac{A_1}{\sqrt{3}\,A_2}\right)\rho(r) - \dfrac{A_3}{\sqrt{3}\,A_2}, \end{cases} \tag{13}$$

where $\rho(r)$ can be obtained in MATLAB using $\rho(r) - \rho(a) + (1/2)(A_1 - \sqrt{3/2}\,A_2)\ln(\rho(r)/\rho(a)) - \sqrt{3/2}\,A_2 \ln(r/a) = 0$, the known material parameters, and $\rho(a) = (1/2)[-(A_1 - \sqrt{3/2}\,A_2) + \sqrt{(C_1 - \sqrt{3/2}\,A_2)^2 - 4A_3}\,]$.

When the plastic zone ($a \le r \le r_p$) begins to appear in the shaft lining, the shaft lining in the elastic zone ($r_p \le r \le b$) can be treated as a new elastic shaft lining subjected to an inner load q (where $r = r_p$) and an external load p (where $r = b$). The components of stress due to these loads can be expressed as

$$\begin{cases} \sigma_r = \dfrac{b^2 r_p^2 (p-q)}{\left(b^2 - r_p^2\right) r^2} + \dfrac{r_p^2 q - b^2 p}{b^2 - r_p^2}, \\ \sigma_\theta = -\dfrac{b^2 r_p^2 (p-q)}{\left(b^2 - r_p^2\right) r^2} + \dfrac{r_p^2 q - b^2 p}{b^2 - r_p^2}. \end{cases} \tag{14}$$

The relationship between the ultimate bearing capacity of the HSHPRCSL, P_b, and the radius of the plastic zone of the shaft wall, r_p, can be obtained using the three-parameter strength criterion, and the radial stress at the interface between the elastic and plastic zones as follows

$$p_b = \frac{\sqrt{\left[4b^2 q - \left(b^2 - r_p^2\right)\alpha\right]^2 - 8\left[2b^4 q^2 - \left(b^2 - r_p^2\right)\left(\sqrt{2}\,b^2 A_1 - \sqrt{3}\,r_p^2 A_2\right)q + A_3\left(b^2 - r_p^2\right)^2\right]} + \left[4b^2 q - \left(b^2 - r_p^2\right)\alpha\right]}{4b^2}, \tag{15}$$

where $\alpha = \sqrt{2}A_1 - \sqrt{3}A_2$.

6. Analysis of Results

6.1. Theoretical Analysis of Ultimate Bearing Capacity of HSHPRCSL. According to the Code for the Design of Concrete Structures [25, 26] with reference to Tables 6 and 7, when the concrete strength grade is between C40 and C80, $K_y = \sigma_y/\sigma_1 = 11.21$—$16.14$, the exact value of which can be calculated by interpolation according to the measured strength grade of the concrete. Because the failure of the shaft lining first occurred on the inner face at the edge of the lining, $f_1 = \sigma_\theta$, $f_2 = \sigma_\theta/2$, $f_1/f_2 = (\sigma_\theta)/(\sigma_\theta/2) = 2$, and $\sigma_{2y}/\sigma_y = f_1/\sigma_y = 1.264$ can be obtained by interpolating the information in Table 8, so $K_{2y} = \sigma_{2y}/\sigma_1 = 14.17$—$20.40$. According to equation (15), if the strength grade of the concrete and the geometry of the shaft lining have already been determined, the relationship between the ultimate bearing capacity P_b of the HSHPRCSL and its plastic zone radius r_p can be determined. Accordingly, the ultimate bearing capacity of each specimen in the model experiment was analysed using the three-parameter strength criterion with the resulting ultimate bearing capacities shown in Table 9. Clearly, the differences between the calculated and experimental results are very small, all less than 8%, indicating that the proposed theoretical equation derived from the three-parameter strength criterion, which has fewer parameters and a simpler functional form than the more complex multiaxial strength theory, can accurately reflect the mechanical properties of an HSHPRCSL structure.

According to the analysis of model test results, the ultimate bearing capacities of the HSHPRCSL models were found to be significantly influenced by the concrete strength to the extent that the ultimate bearing capacity of a HSHPRCSL is most effectively improved by increasing the strength of the concrete during the design stage. To analyse the degree of correlation between the experimentally derived fitted equation and the theoretically derived equation based on the three-parameter strength criterion for the ultimate bearing capacity of the shaft lining, specimens with thickness-diameter ratios of $\lambda = 0.216$ and 0.201 for A-1–A-3 and A-4–A-6, respectively, were compared separately. The ultimate bearing capacities of the HSHPRSCL specimens constructed of C60–C80 concrete for thickness-diameter ratios of $\lambda = 0.216$ and 0.201 were then obtained as shown in Figures 13 and 14, respectively.

From Figures 13 and 14, it can be seen that the trend law of the ultimate bearing capacity with the change in concrete compressive strength as determined by the three-parameter strength criterion is the nearly the same as that of the fitted curve, with both approximating a linear distribution. Figure 13 shows that when the inner radius of the shaft lining $a = 380.5$ mm, the outer radius $b = 462.5$ mm and the thickness-diameter ratio $\lambda = 0.216$, as the concrete strength grade increases by 5 MPa within the range of C60–C80, the ultimate bearing capacity of the shaft lining obtained by the fitted curve increases by approximately 2.4 MPa, while the ultimate bearing capacity based on the three-parameter strength criterion increases about 2.67 MPa. Figure 14 shows that when the inner radius of the shaft lining $a = 385$ mm, the outer radius $b = 462.5$ mm and the thickness-diameter ratio $\lambda = 0.201$, as the concrete strength grade increases by 5 MPa within the range of C60–C80, the ultimate bearing capacity of the shaft lining obtained by the fitted curve increases by approximately 2.25 MPa, while the ultimate bearing capacity based on the three-parameter strength criterion increases by about 2.44 MPa.

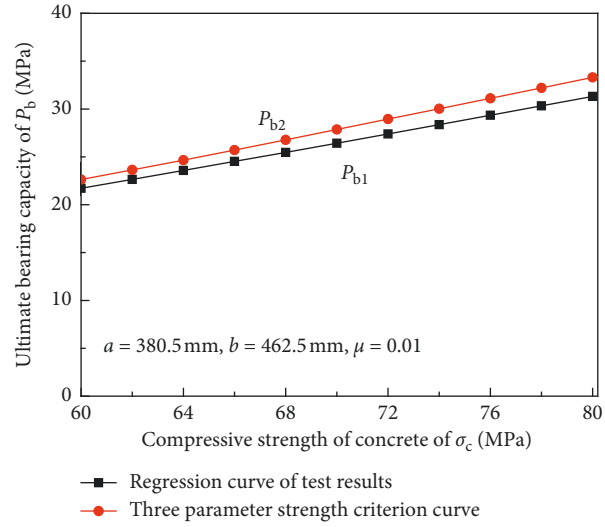

Figure 13: The relationship between ultimate bearing capacity and compressive strength when $\lambda = 0.216$.

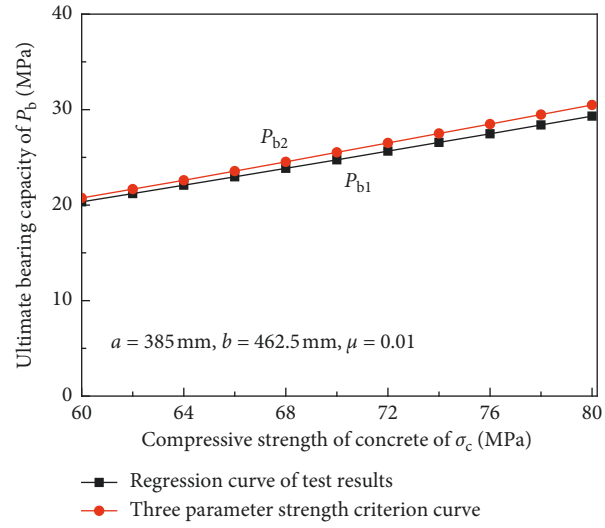

Figure 14: The relationship between ultimate bearing capacity and compressive strength when $\lambda = 0.201$.

The above analysis demonstrates that the difference between the ultimate bearing capacity of the HSHPRCSL calculated using the proposed equation based on the three-parameter strength criterion and calculated using the fitting equation based on experimental results is very small, with errors around about ±5%. Thus, the calculation of the ultimate bearing capacity of HSHPRCSL by equations (8)

and (15) is reliable, providing a basis for the design of HSHPRCSL structures.

6.2. Finite Element Analysis of Ultimate Bearing Capacity of HSHPRCSL. It is well known that reasonable and accurate numerical approach could be implemented as an alternative to costly and time-consuming full-scale experimental tests, allowing an extensive parametric investigation of composite joints and possible design optimizations [28]. In order to understand the actual ultimate bearing capacity of the shaft lining with the same strength under the boundary conditions of engineering practices, the finite element numerical simulation method is used to further analyse the ultimate bearing capacity of the shaft lining.

In the finite element model, the concrete is simulated by SOLID65 three-dimensional solid element, the steel bar is simulated by LINK8 bar element, and the reinforced-concrete separated model is adopted. Displacement coordination is achieved by sharing joint between concrete elements and steel elements. The constitutive relationship of concrete is determined by the multilinear kinematic hardening model (bilinear kinematic), as well as the uniaxial compressive test results of HSHPC blocks. The failure criterion of concrete is Willam and Warnke's five-parameter failure criterion [29]. The bilinear kinematic hardening model is adopted for steel bars, and Mises criterion is used for its yield. Vertical constraints are applied to the upper and lower surfaces of the model, and uniform surface loads are applied to the outer surface of the model according to the loading history of the test. The network partition of the finite element model is shown in Figure 15. Specific physical and mechanical parameters of concrete and steel bar are shown in Tables 10 and 11.

Through finite element calculation, the ultimate bearing capacity of 8 HSHPRCSLs is obtained. From Table 9, it can be seen that the finite element calculation results of ultimate bearing capacity of HSHPRCSL are slightly higher than those of model tests and theoretical formulas. The reason is that the constraints of the finite element model fully reflect the three-dimensional compressive state of the shaft lining, and the ultimate compressive strength of concrete will be greatly improved under the three-dimensional compressive state, which cannot be truly reflected in the test. Generally speaking, the errors are all less than 12%, which verifies the rationality of the finite element model. It is further explained that the research carried out in this paper can provide a basis for the design of high-strength and high-performance concrete shaft lining.

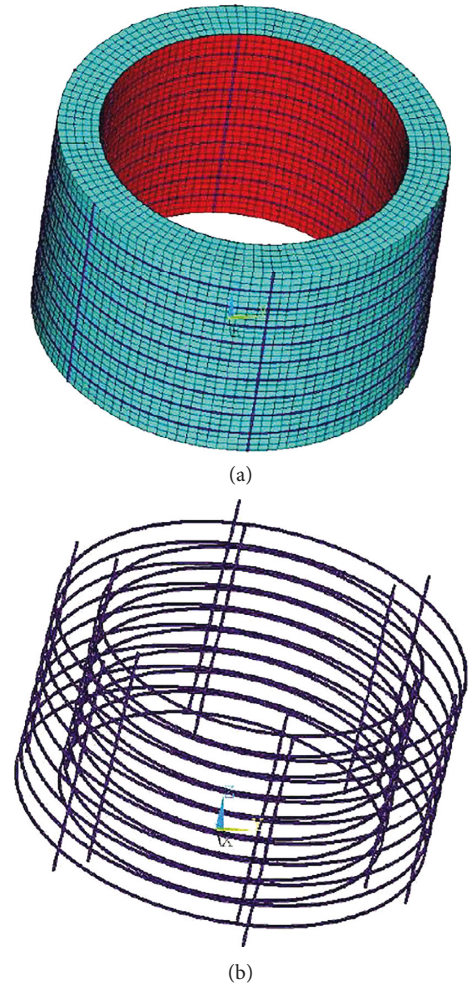

Figure 15: Finite element model of HSHPRCSL.

7. Conclusions

In this study, a series of high-strength, high-performance concrete (HSHPRC) mix tests were first conducted to determine the optimal mix ratio for use in deep freezing shaft linings. Then, a series of high-strength, high-performance reinforced concrete shaft lining (HSHPRCSL) models were tested to determine their mechanical properties and failure characteristics. And then, a theoretical analysis based on the three-parameter strength criterion was undertaken to determine the ultimate bearing capacity of the HSHPRCSL models, providing analytical expressions for elastic and plastic zone radii, stress, and load. Finally, the finite element analysis method is used to verify the abovementioned results. The following conclusions were obtained:

(1) According to the special curing environment and construction conditions to which deep freezing shaft linings are subjected, an optimised concrete mix was proposed for concrete strengths in the range of C60 to C80, providing important information to promote improved design and construction of deep alluvium freezing shaft linings.

(2) When the HSHPRCSL models ruptured, large chunks of concrete were observed to fall, inclined broken cracks appeared, plastic bending of the circumferential reinforcement occurred along the failure surface, and compressive-shear failure occurred with an angle between the failure surface and the maximum principle stress of 25–30°.

(3) Results of the HSHPRCSL model tests indicated a high ultimate bearing capacity. The factors that

Table 10: The force parameter table of concrete.

Model	E ($\times 10^4$ MPa)	Poisson ratio	σ_f (MPa)	σ_{cm} (MPa)	σ_t (MPa)	β_t	β_c
A-1	3.66	0.2	39.2	65.3	7.18	0.45	0.9
A-2	3.72	0.2	43.3	72.2	8.10	0.45	0.9
A-3	3.77	0.2	46.1	76.8	8.35	0.45	0.9
A-4	3.59	0.2	40.7	67.9	7.45	0.45	0.9
A-5	3.67	0.2	44.5	74.2	8.21	0.45	0.9
A-6	3.75	0.2	47.6	79.3	8.42	0.45	0.9
A-7	3.62	0.2	37.3	62.2	6.71	0.45	0.9
A-8	3.78	0.2	47.0	78.3	8.39	0.45	0.9

Note: E is the modulus of elasticity; σ_f is the yield stress; σ_t is the uniaxial tensile strength of concrete; β_t is the shear transfer coefficient when cracks open; and β_c is the shear transfer coefficient when the crack closes.

Table 11: The force parameter table of rebar.

E ($\times 10^5$ MPa)	Poisson ratio	σ_f (MPa)
2.1	0.3	340

influenced the ultimate bearing capacity were, in order of decreasing influence, the ultimate uniaxial compressive strength of the concrete, the thickness-diameter ratio, and the reinforcement ratio. Under a uniform externally applied load, when the concrete strength grade was increased by 10 MPa, the ultimate bearing capacity of the model increased by 6.29 MPa. For the same concrete strength grade, an increase in the reinforcement ratio from 0.3% to 0.8% only improved the ultimate bearing capacity of the shaft lining by about 0.85 MPa.

(4) The theoretical HSHPRCSL ultimate bearing capacities, calculated based on the three-parameter strength criterion, were basically consistent with the experimental results, showing an error of less than 8%. Clearly, the proposed method for the theoretical calculation of the ultimate bearing capacity of HSHPRCSL structures is reliable, providing a theoretical basis for the design of HSHPRCSL structures in deep alluvium freezing wells.

(5) Due to the constraints of the finite element model fully reflecting the three-dimensional compression state of the borehole lining, the finite element calculation results of the ultimate bearing capacity of HSHPRCSL are slightly higher than those of the model test and theoretical formula. However, the errors are less than 12%, which verifies the rationality of the finite element model.

Data Availability

The data used to support the findings of this study are available from the corresponding author upon request.

Conflicts of Interest

The authors declare that there are no conflicts of interest regarding the publication of this paper.

Acknowledgments

This work was financially supported by the National Natural Science Foundation of China (Grant nos. 51374010, 51474004, 51874005, 51878005, and 51804006) and The Key project of Anhui Provincial Natural Science Research in Colleges and Universities (Grant nos. KJ2010A094 and KJ2011A093).

References

[1] Y. Yao, H. Cheng, C. Rong et al., "Analysis and prediction of vertical shaft freezing pressure in deep alluvium based on RBF fuzzy neural network model," *Journal of Mining & Safety Engineering*, vol. 33, pp. 70–76, 2016, in Chinese.

[2] G. Spagnoli, P. Oreste, and L. Lo Bianco, "New equations for estimating radial loads on deep shaft linings in weak rocks," *International Journal of Geomechanics*, vol. 16, no. 6, article 06016006, 2016.

[3] Z. Yao, H. Cheng, and J. Yang, "Experimental study on mechanical properties of high strength reinforced concrete shaft lining in deep alluvium," *Journal of China Coal Society*, vol. 29, pp. 167–171, 2004, in Chinese.

[4] H. Song, H. Cheng, and Z. Yao, "An experimental research of large volume high-strength and high-performance concrete in deep frozen shaft lining and its application," *West, China Exploration Engineering*, vol. 18, pp. 154–156, 2006, in Chinese.

[5] H. Lü and G. Cui, "Mechanical mechanism of shaft lining structure fracture in thick alluvium," *Journal of China University of Mining and Technology*, vol. 28, pp. 539–543, 1999, in Chinese.

[6] X. Chen and W. Yang, "Curing monolayer freezing shaft lining," *Journal of China University of Mining and Technology*, vol. 39, pp. 201–207, 2010, in Chinese.

[7] J. Yang, "Failure and strength characteristics of the concrete shaft lining," *Journal of China Coal Society*, vol. 23, pp. 246–251, 1998, in Chinese.

[8] L. Liao, A. de la Fuente, S. Cavalaro, and A. Aguado, "Design procedure and experimental study on fibre reinforced concrete segmental rings for vertical shafts," *Materials & Design*, vol. 92, pp. 590–601, 2016.

[9] T. Majcherczyk, Z. Niedbalski, and D. Wałach, "Variations in mechanical parameters of rock mass affecting shaft lining/zmiany parametrów mechanicznych górotworu I ich wpływ na obudowę szybową," *Archives of Mining Sciences*, vol. 58, no. 3, pp. 629–642, 2013.

[10] G. Tiberti, F. Minelli, and G. Plizzari, "Reinforcement optimization of fiber reinforced concrete linings for conventional

tunnels," *Composites Part B: Engineering*, vol. 58, pp. 199–207, 2014.

[11] Y. Wang, J. Huang, J. Li et al., "Early-stage strength growth of high-strength concrete in outer freezing shaft walls," *Journal of China University of Mining and Technology*, vol. 37, pp. 595–598, 2008, in Chinese.

[12] Z. Yao, H. Cheng, and W. Sun, "Testing studies on the structure of high strength composite shaft wall in deep soil layer," *Rock and Soil Mechanics*, vol. 24, pp. 739–743, 2003, in Chinese.

[13] Z. Yao, H. Cheng, and C. Rong, "Experimental study on composite shaft Lining of inner steel plate cylinder and high strength reinforced concrete in deep frozen shaft," *Chinese Journal of Rock Mechanics and Engineering*, vol. 27, pp. 153–158, 2008, in Chinese.

[14] C. Rong, X. Wang, and H. Cheng, "Research on mechanical characteristics of high-strength reinforced concrete shaft lining in deep alluvium," *Chinese Journal of Rock Mechanics and Engineering*, vol. 27, pp. 2841–2847, 2008, in Chinese.

[15] Z. Guo and C. Wang, "Investigation of strength and failure criterion of concrete under multi-axial stresses," *China Civil Engineering Journal*, vol. 24, pp. 1–13, 1991, in Chinese.

[16] Z.-s. Yao, H. Chang, and C.-x. Rong, "Research on stress and strength of high strength reinforced concrete drilling shaft lining in thick top soils," *Journal of China University of Mining and Technology*, vol. 17, no. 3, pp. 432–435, 2007.

[17] R. Ritter and M. Curbach, "Material behavior of ultra-high-strength concrete under multiaxial stress states," *ACI Materials Journal*, vol. 112, no. 5, pp. 641–651, 2015.

[18] K. Speck and M. Curbach, "Ein einheitliches dreiaxiales Bruchkriterium für alle Betone," *Beton und Stahlbetonbau*, vol. 105, no. 4, pp. 233–243, 2010.

[19] B. Xu and X. Liu, *Applied Elastic-Plastic Mechanics*, Tsinghua University Press, Beijing, China, 1995, in Chinese.

[20] Y. Zhang and M. Lu, "Three-parameter failure criterion for plain concrete," *Journal of Shanghai Jiaotong University*, vol. 24, pp. 62–88, 1990, in Chinese.

[21] P. V. Lade, "Three-parameter failure criterion for concrete," *Journal of the Engineering Mechanics Division*, vol. 108, pp. 850–863, 1982.

[22] S. A. B. da Fontoura, "Lade and modified lade 3D rock strength criteria," in *The ISRM Suggested Methods for Rock Characterization, Testing and Monitoring: 2007-2014*, R. Ulusay, Ed., Springer International Publishing, Cham, Switzerland, 2015.

[23] L. I. Sedov, M. Friedman, and R. E. Street, *Similarity and Dimensional Methods in Mechanics*, Mir Publishing, Moscow, Russia, 1982.

[24] J. Dong, J. Yang, G. Yang et al., "Research on similar material proportioning test of model test based on orthogonal design," *Journal of China Coal Society*, vol. 37, pp. 44–49, 2012, in Chinese.

[25] The National Standards Compilation Group of the People's Republic of China, *GB50010–2010 Code for Design of Concrete Structures*, China Architecture and Building Press, Beijing, China, 2010, in Chinese.

[26] American Concrete Institute, *Building Code Requirements for Structural Concrete and Commentary, ACI 318R-11*, American Concrete Institute, Farmington Hills, MI, USA, 2011.

[27] X. Li, C. Rong, and H. Cheng, "Mechanical properties of high-strength concrete shaft lining based on three-parameter strength criterion," *Journal of Guangxi University (Natural Science Edition)*, vol. 41, pp. 308–316, 2016, in Chinese.

[28] C. Amadio, C. Bedon, M. Fasan, and M. R. Pecce, "Refined numerical modelling for the structural assessment of steel-concrete composite beam-to-column joints under seismic loads," *Engineering Structures*, vol. 138, pp. 394–409, 2017.

[29] C. Rong and H. Cheng, "Study on mechanical characteristics of reinforced concrete arc shaft wall in frozen shaft," *Rock and Soil Mechanics*, vol. 27, pp. 193–198, 2006, in Chinese.